



Article

Drug-Releasing Antibacterial Coating Made from Nano-Hydroxyapatite Using the Sonocoating Method

Khaled AbouAitah ^{1,2,*} , Monika Bil ³, Elzbieta Pietrzykowska ^{1,4}, Urszula Szałaj ^{1,4} , Damian Fudala ¹, Bartosz Woźniak ¹, Justyna Nasiłowska ^{5,6}, Anna Swiderska-Sroda ¹, Maciej Lojkowski ⁴, Barbara Sokołowska ^{5,6} , Wojciech Swieszkowski ⁴ and Witold Lojkowski ^{1,*}

- ¹ Laboratory of Nanostructures and Nanomedicine, Institute of High Pressure Physics, Polish Academy of Sciences, 29/37 Sokolowska Street, 01142 Warsaw, Poland; e.pietrzykowska@labnano.pl (E.P.); u.szalaj@labnano.pl (U.S.); d.fudala@labnano.pl (D.F.); woźniakbartoszz@gmail.com (B.W.); a.swiderska-sroda@labnano.pl (A.S.-S.)
 - ² Medicinal and Aromatic Plants Research Department, Pharmaceutical and Drug Industries Research Division, National Research Centre (NRC), Dokki, Giza 12622, Egypt
 - ³ Centre for Advanced Materials and Technologies, Warsaw University of Technology, Poleczki 19, 02822 Warsaw, Poland; monika.bil@pw.edu.pl
 - ⁴ Faculty of Materials Science and Engineering, Warsaw University of Technology, 141 Woloska Street, 02507 Warsaw, Poland; Maciej.Lojkowski.dokt@pw.edu.pl (M.L.); wojciech.swieszkowski@pw.edu.pl (W.S.)
 - ⁵ Department of Microbiology, Prof. Waclaw Dąbrowski Institute of Agriculture and Food Biotechnology–State Research Institute, 36 Rakowiecka Street, 02532 Warsaw, Poland; justyna.nasilowska@ibprs.pl (J.N.); barbara.sokolowska@ibprs.pl (B.S.)
 - ⁶ High Pressure Food and Soft Matter Processing Group, Institute of High-Pressure Physics, Polish Academy of Sciences, 29/37 Sokolowska Street, 01142 Warsaw, Poland
- * Correspondence: k.abouaitah@labnano.pl (K.A.); w.lojkowski@labnano.pl (W.L.); Tel.: +48-22-6325010 (W.L.); Fax: +48-22-632-4218 (W.L.)



Citation: AbouAitah, K.; Bil, M.; Pietrzykowska, E.; Szałaj, U.; Fudala, D.; Woźniak, B.; Nasiłowska, J.; Swiderska-Sroda, A.; Lojkowski, M.; Sokołowska, B.; et al. Drug-Releasing Antibacterial Coating Made from Nano-Hydroxyapatite Using the Sonocoating Method. *Nanomaterials* **2021**, *11*, 1690. <https://doi.org/10.3390/nano11071690>

Academic Editors: Vi-Khanh Truong and Constantine D. Stalikas

Received: 15 May 2021
Accepted: 14 June 2021
Published: 28 June 2021

Publisher's Note: MDPI stays neutral with regard to jurisdictional claims in published maps and institutional affiliations.



Copyright: © 2021 by the authors. Licensee MDPI, Basel, Switzerland. This article is an open access article distributed under the terms and conditions of the Creative Commons Attribution (CC BY) license (<https://creativecommons.org/licenses/by/4.0/>).

Abstract: Medical implant use is associated with a risk of infection caused by bacteria on their surface. Implants with a surface that has both bone growth-promoting properties and antibacterial properties are of interest in orthopedics. In the current study, we fabricated a bioactive coating of hydroxyapatite nanoparticles on polyether ether ketone (PEEK) using the sonocoating method. The sonocoating method creates a layer by immersing the object in a suspension of nanoparticles in water and applying a high-power ultrasound. We show that the simple layer fabrication method results in a well-adhering layer with a thickness of 219 nm to 764 nm. Dropping cefuroxime sodium salt (Cef) antibiotic on the coated substrate creates a layer with a drug release effect and antibacterial activity against *Staphylococcus aureus*. We achieved a concentration of up to 1 mg of drug per cm² of the coated substrate. In drug release tests, an initial burst was observed within 24 h, accompanied by a linear stable release effect. The drug-loaded implants exhibited sufficient activity against *S. aureus* for 24 and 168 h. Thus, the simple method we present here produces a biocompatible coating that can be soaked with antibiotics for antibacterial properties and can be used for a range of medical implants.

Keywords: antibacterial coating; hydroxyapatite nanoparticles; sonocoating; PEEK implants; cefuroxime sodium salt antibiotic; drug release; *Staphylococcus aureus* bacteria

1. Introduction

Coating the surface of medical implants to provide biocompatibility, bioactivity, antibacterial, anticancer, and bone-growth properties is a well-established technology [1]. Implantation leads to a risk of infection caused by bacteria attached to the implant surface. The risk is particularly high for patients with low systemic and local immunity, as these bacteria may invade the circulation or remain in the tissues surrounding the inserted implant [2]. Among other bacteria, *Staphylococcus*, *Enterobacteriaceae*, and *Pseudomonas* cause considerable medical problems because they can attach to the implant surface, producing a

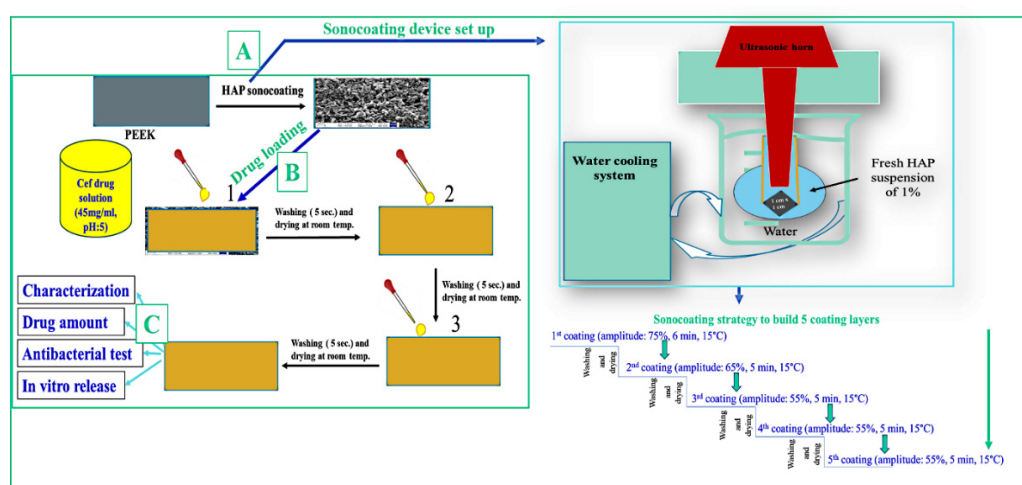
biofilm [3]. In the case of infection with pathogens such as the Gram-positive *Staphylococcus aureus*, site infections occur in >5% of medical implant and device implantations [4]. The critical time of colony formation by bacteria after the placement of any implant is from a few hours up to 72 h [5]. Many studies have shown that the stage of bacterial attachment and biofilm formation lasts from 12 to 24 h, and proliferation and maturation of the biofilm occurs from 36 to 72 h [5,6]. After the biofilm is established, bacterial cells can spread in the tissues, causing chronic infections. Thus, preventing biofilm formation is essential to reducing the risk of post-operative infection [6]. Consequently, there are different strategies toward bacterial biofilm, including surface modification of medical devices/implants [7], small molecule biofilm inhibitors [8], biofilm dispersal agents [9], and antibacterial coatings [10,11]. Antibacterial coatings may prevent biofilm formation and prevent inflammation [2,12] and are employed to locally deliver antibiotic drugs and therapeutic agents for short- (few hours or days) or long-acting antibacterial effects (days and weeks) [13].

In this context, phosphate materials, especially hydroxyapatite phases, have been considered as coating materials for bone implants because they are similar to the mineral components of the bone tissue and their biocompatibility [14–16]. Micro and nanoparticles of hydroxyapatite (nanoHAP) have been used for coatings to enhance bone formation and in drug delivery systems to carry drugs and deliver growth factors and proteins [16–21]. The local delivery and release of drugs by a nanoHAP coating permits highly efficient targeting of the infected area with reduced cytotoxicity [18,19,22]. The layer properties may strongly depend on such properties of the synthesized particles as specific surface area and particle size. For example, Szalaj, et al. demonstrated that nanoparticle size strongly changes the kinetics and efficiency of water adsorption, which is related to the specific surface area [23]. Several attempts to achieve long-term antibacterial actions using antibiotic-loaded HAP [18,20,24] or HAP with antibacterial doping [25,26] have been reported. However, a coating with short-term antibacterial action that enhances subsequent bone growth is still a challenge.

Polyether ether ketone (PEEK) is a candidate material for implants because of its chemical resistance and its mechanical properties matching that of the bone and radiolucency [21,27]. PEEK possesses an elastic modulus (3.2 GPa) between that of cortical (15–30 GPa) and cancellous bone (0.5–1.5 GPa) [21]. In addition, PEEK has a bio-inert and hydrophobic nature, which results in poor osseointegration characteristics [27,28]. Therefore, coatings and surface modifications have been developed that improve its bioactive properties and increase its osseointegration properties. One of these techniques is to coat the PEEK with hydroxyapatite.

Several methods have been developed for coating PEEK with hydroxyapatite [29–31]. Johansson, et al. [21] reported nano-sized coating of hydroxyapatite crystal on PEEK implants to enhance bone formation. However, this method requires many steps and high temperature, and there is an organic residue. Other methods include electrostatic and covalent attachment [32], electrophoretic deposition [18], electrochemical deposition [33], biomimetic precipitation [34], physical vapor deposition techniques [35,36], and plasma spraying [37], among others. However, the coatings obtained using these methods have a thickness measured in micrometers and a non-porous structure. Thus, another technique is required to produce thin nanoscale layers with a porous structure able to carry the antibacterial drugs. In the last decade, a sonochemical technique has been developed for creating antibacterial coatings of metal nanoparticles on different surfaces, mostly textiles for medical applications [38–41]. We attempted to use this method to obtain a nanoHAP coating on the PEEK surface. To coat the object, it is immersed in a nanoparticle suspension in water. Treatment of the suspension with high-power ultrasound waves leads to attachment of the nanoparticles to the surface of the object. This is a green chemistry approach as no chemicals are used. The advantage of this method is that it is a single, easy step at low cost and low temperature. The mechanism by which the nanoHAP layer is created on a polymer was recently described by Wozniak, et al. [42]. The nanoHAP layer(s)

is grown laterally in a dendrite-like pattern on the surface. Sonocoating with nanoHAP on bone regrowth scaffolds has also been shown to enhance bone regeneration [16]. Therefore, sonocoating is considered an excellent approach for obtaining nanoHAP layers on various substrates by means of green chemistry. Therefore, in the current study, we sonocoated nanoHAP onto PEEK substrates to create a biocompatible layer (Scheme 1) with a potential to stimulate bone growth while absorbing antibacterial drugs. We applied antibiotic cefuroxime sodium salt (Cef) and carried out drug release tests. We selected Cef as a model antibiotic, a second-generation cephalosporin, because it is efficient and has broad applications against both Gram-negative and Gram-positive micro-organisms [43–45]. The sodium salt form of Cef has been used for a long time due to its solubility, injection application, various purposes in clinical practice, and sparse drug allergy in patients [46,47]. For these reasons, it is frequently used as a prophylaxis in total joint replacement and an antibiotic in orthopedic surgery [48–50].



Scheme 1. Schematic of controlled nanolayer coating and antibacterial evaluation. (A) Preparation method for one to five iterations of coating to obtain a nanolayer thickness using optimized parameters. (B) Drug loading method. (C) Characterized materials and their antibacterial effects.

2. Materials and Methods

2.1. Synthesis of nanoHAP Solutions for Coating

GoHAPTM, developed at the Institute of High Pressure Physics, Polish Academy of Sciences (IHPP PAS), were the nanoHAP used for sonocoating. GoHAP1 and GoHAP3 were selected because they exhibit different particle sizes and specific surface areas. The procedure has been described in detail elsewhere [16,23,51]. GoHAP1 particles (approximately 9 nm in size with a specific surface area of $206 \pm 1 \text{ m}^2/\text{g}$) and GoHAP3 particles (approximately 16 nm in size with a specific surface area $149 \pm 1 \text{ m}^2/\text{g}$) were synthesized using the MSS2 microwave reactor (manufactured by IHPP PAS in collaboration with Łukasiewicz Research Network—The Institute for Sustainable Technologies, Radom, Poand) at 3 kW and 2.45 GHz [52].

2.2. Sonocoating of PEEK Implants

The PEEK medical implant substrate (Goodfellow Cambridge Limited, Huntingdon, UK) was cut into 1 cm^2 plates and cleaned in ethanol for 15 min using a water bath sonicator (Elma water bath sonicator, Singen, Germany). For sonocoating, we used suspensions of the two different types of GoHAPTM at a concentration of 1 wt % in distilled water. Coating was performed in subsequent steps for one to five iterations under controlled conditions as shown in Scheme 1A. The sonocoating process used a $\varnothing 13 \text{ mm}$ diameter titanium ultrasonic horn at 20 kHz frequency. The VCX 750 generator (Sonics, Newtown, CT, USA), operating at 750 W, provided ultrasonic energy. During coating, a 75% vibration amplitude

was applied for 6 min, and then the PEEK substrate was washed in deionized water for 5 s under magnetic stirring. The samples were left at room temperature to dry. To increase the layer thickness, the coating procedure was repeated with smaller amplitudes and shorter times (second cycle: 65% and 5 min; third to fifth cycle: 55% for 5 min). For each iteration, a fresh suspension was prepared. Samples were dried between the coatings.

2.3. Incorporating the Antibacterial Drug in Sonocoated nanoHAP

Geuli, et al. [18] first loaded antibiotic drugs on HAP nanoparticles and then fabricated the antibacterial coating. However, this technique may affect the chemical structure of the used drugs (e.g., use of high temperature for fabrication process, strong solvents, etc.). Here, we used the simple drop-by-drop method to saturate the coated surface. The drug solution (45 mg/mL) was initially adjusted to an acidic pH of 5. The prepared solution was applied by dropping the equivalent of 50 μ L onto the surface of the dried GoHAP-coated samples, which were then washed with deionized water under medium stirring (300 rpm) for 5 s and left at room temperature to dry. The procedure was repeated three times. The obtained samples were named PEEK-HAP1-Cef and PEEK-HAP3-Cef.

2.4. Determination of the Amount of Loaded Drug

To measure the drug loading, we extracted the loaded drug by placing the samples in a glass bottle containing deionized water (3 mL) and sonicating it for 15 min (Elma water bath sonicator, Singen, Germany). The solution was collected, and the procedure repeated a second time to ensure that all drug was extracted. Next, the collected sonicated solution (6 mL) was filtered using a syringe filter (0.45 μ m) to remove any nanoHAP particles that could influence the UV–Vis measurements. The quantitative determination was performed by measuring the samples at 275 nm on an Evolution™ 60 UV–Visible spectrophotometer (Thermo Scientific, Pittsburgh, PA, USA) using a standard curve prepared for Cef. Each measurement was replicated five times.

2.5. In Vitro Drug Release Study

The PEEK-HAP1-Cef and PEEK-HAP3-Cef samples were placed separately in glass bottles with a screw cap and 3 mL of phosphate-buffered saline (PBS) buffer was added. Next, the samples were placed in an immersion circulator with a submersible multi-position stirrer at 37 °C and 150 rpm (IKA Poland, Warsaw, Poland). At specified time points (from 2 h to 150 h), the entire volume of PBS was sampled and stored in vials at 4 °C until UV–Vis analysis. The removed sample was replaced with a fresh release medium. The solutions were measured by using the Evolution™ 60 UV–Visible Spectrophotometer at 275 nm. The Cef concentration at each time point was determined based on the previously prepared calibration curve. Three measurements were performed for each sample. The cumulative drug release was calculated based on the following equations:

$$\% \text{ of mass released at time } t = (\text{mass}(t) / \text{total mass of Cef in the coated substrate}) \times 100 \quad (1)$$

$$\text{cumulative release } \% = \text{mass}(t - 1) + \text{mass}(t) \text{ for current measurement} \quad (2)$$

where t is the percentage release at the time of measurement and $t - 1$ is the percentage of released drug at the previous time point.

2.6. Characterization Techniques

Several characterization techniques were used to investigate the nanolayer. Scanning electron microscopy (SEM) was performed using an Ultra Plus Scanning Electron Microscope (Zeiss, Jena, Germany) to observe the morphology of the layer (s) of nanoHAP on the surface and the thickness of the coated layer (s). The coated PEEK pellets were fractured in liquid nitrogen. The coat thickness was determined from SEM images using the Gwyddion software (version 2.28, Brno, Czech Republic) [42]. The pore size distribution of the coatings was analyzed in an Excel calculation program after SEM imaging.

Fourier transform infrared (FTIR) spectroscopy was performed to determine the functional groups before and after nanoHAP coating and drug loading. The Bruker Optics Tensor 27 FTIR instrument (Bruker Corporation, Billerica, MA, USA) was equipped with an attenuated total reflectance (Platinum ATR-Einheit A 255). For surface topography, atomic force microscopy (AFM) images were obtained by MFP-3D-Bio (Asylum Research, Oxford Instruments, High Wycombe, UK). We tested the wetting angle using an OCA 20 goniometer (DataPhysics Instruments GmbH, Filderstadt, Germany), and measured the contact angle by applying a drop of deionized water and immediately measuring.

2.7. Assessment of Antimicrobial Activity

The antimicrobial activity was determined by the inhibition zone method and evaluated against *S. aureus* ATCC 25923. In a typical experiment, 100 μL of the overnight culture ($\sim 10^8$ cfu/mL) in Tryptone Soy Broth (TSB; Biokar Diagnostics, Beauvais, France) was spread onto Tryptone Soy Agar (TSA; Biokar Diagnostics, Beauvais, France). The coated PEEK-HAP1 containing Cef was placed on the prepared agar plates and incubated at 37 °C. A plate with only *S. aureus* ATCC 25923 and a plate with *S. aureus* ATCC 25923 and PEEK-HAP1 without antibiotic were incubated as controls. The inhibition zones were measured every 24 h for 11 days. Studies were performed in triplicate.

Broth dilution tests were carried out in TSB by measuring the optical density (OD) at 600 nm using NanoDrop ND-1000 UV-Vis (NanoDrop Technologies, Wilmington, DE, USA). For this purpose, 10 μL of the overnight culture of *S. aureus* ATCC 25923 in TSB was transferred to 3 mL of new TSB with PEEK-HAP1 and PEEK-HAP1-Cef. As a control, TSB with only *S. aureus* ATCC 25923 was incubated. For all samples, incubation was 37 °C for 7 days. All experiments were performed in triplicate.

For the broth dilution method with changing broth, 10 μL of the overnight culture of *S. aureus* ATCC 25923 in TSB was transferred to 3 mL of new TSB with PEEK-HAP-Cef. TSB with only *S. aureus* ATCC 25923, or *S. aureus* ATCC 25923 and PEEK-HAP1 were incubated as controls. All samples were incubated for 10 h at 37 °C. After measuring the OD, the broth was poured out and the samples washed with 3 mL of PBS (POCH, Gliwice, Poland). We then added new 3 mL portions of TSB with 10 μL *S. aureus* ATCC 25923. The actions were repeated after another 14 and 24 h. Studies were performed in triplicate.

2.8. Statistical Analysis

Significant differences were evaluated by one-way analysis of variance (ANOVA) with the least significant difference at $p < 0.05$ [53].

3. Results and Discussion

3.1. Microscopic Characterization

Figure 1 shows the coatings created with GoHAP1 and GoHAP3 on PEEK. The images show changes in the layer structure with each coating iteration for both GoHAP1 and GoHAP3. Using a high amplitude at the beginning and a low amplitude with shorter time in the next iteration (Scheme 1A) prevented damage and cracking of the layers, achieving a thickness of up to 700 nm. It is clear that the creation of the first, second, and third layers was associated with the appearance of some “islands”, whereas more even coverage was observed with the fourth and fifth coatings (especially when observed by the in-lens detector on the left). The coating thickness increased from the first to fifth layer. It seems that coating with GoHAP3 led to a more homogeneous layer compared to GoHAP1. In the latter case, a higher tendency to form islands was observed. In addition, the GoHAP layer had a porous structure when observed by the SE2 detector (Figure 2).

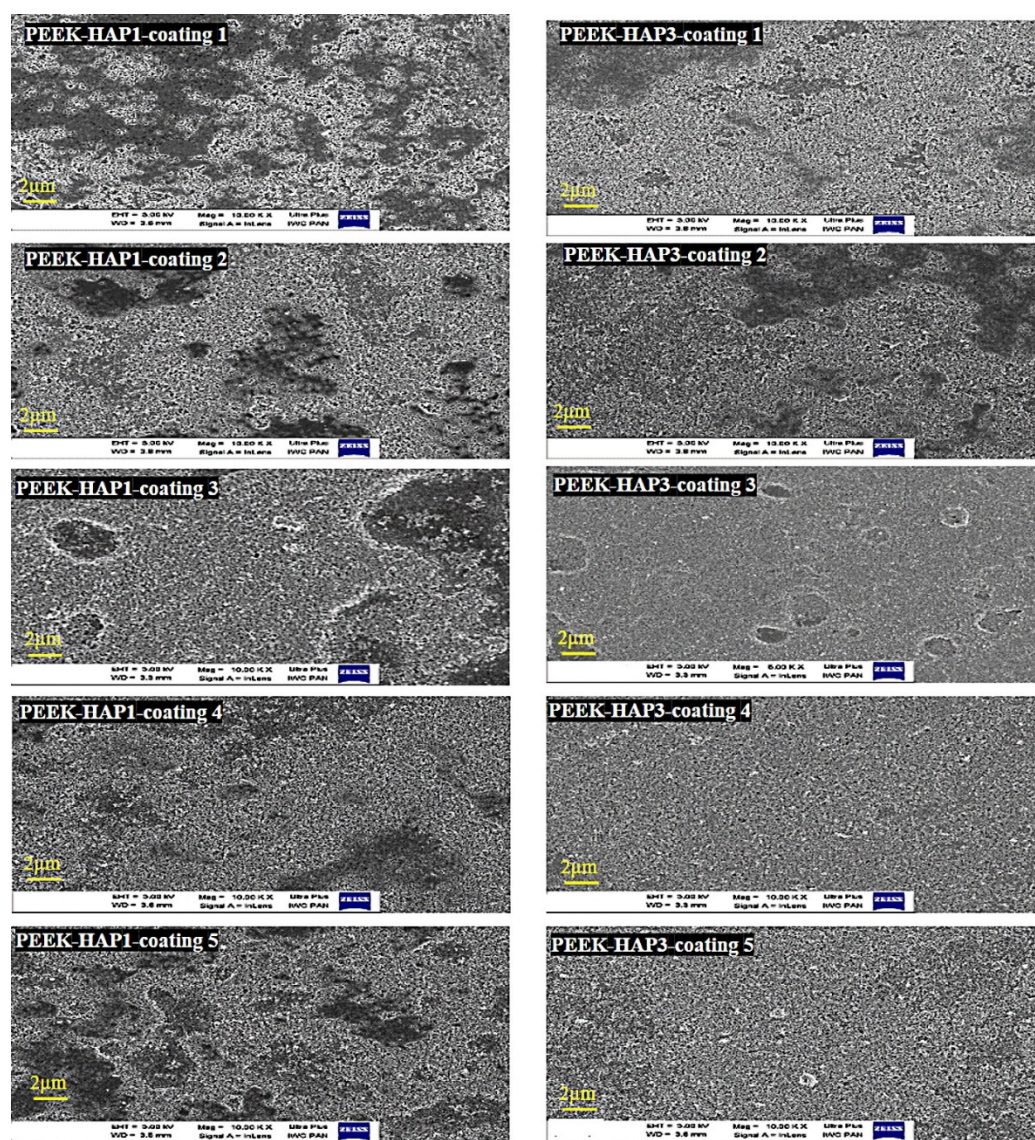


Figure 1. FE-SEM of the morphology of the GoHAP1 and GoHAP3 nanolayers on PEEK in five iterations.

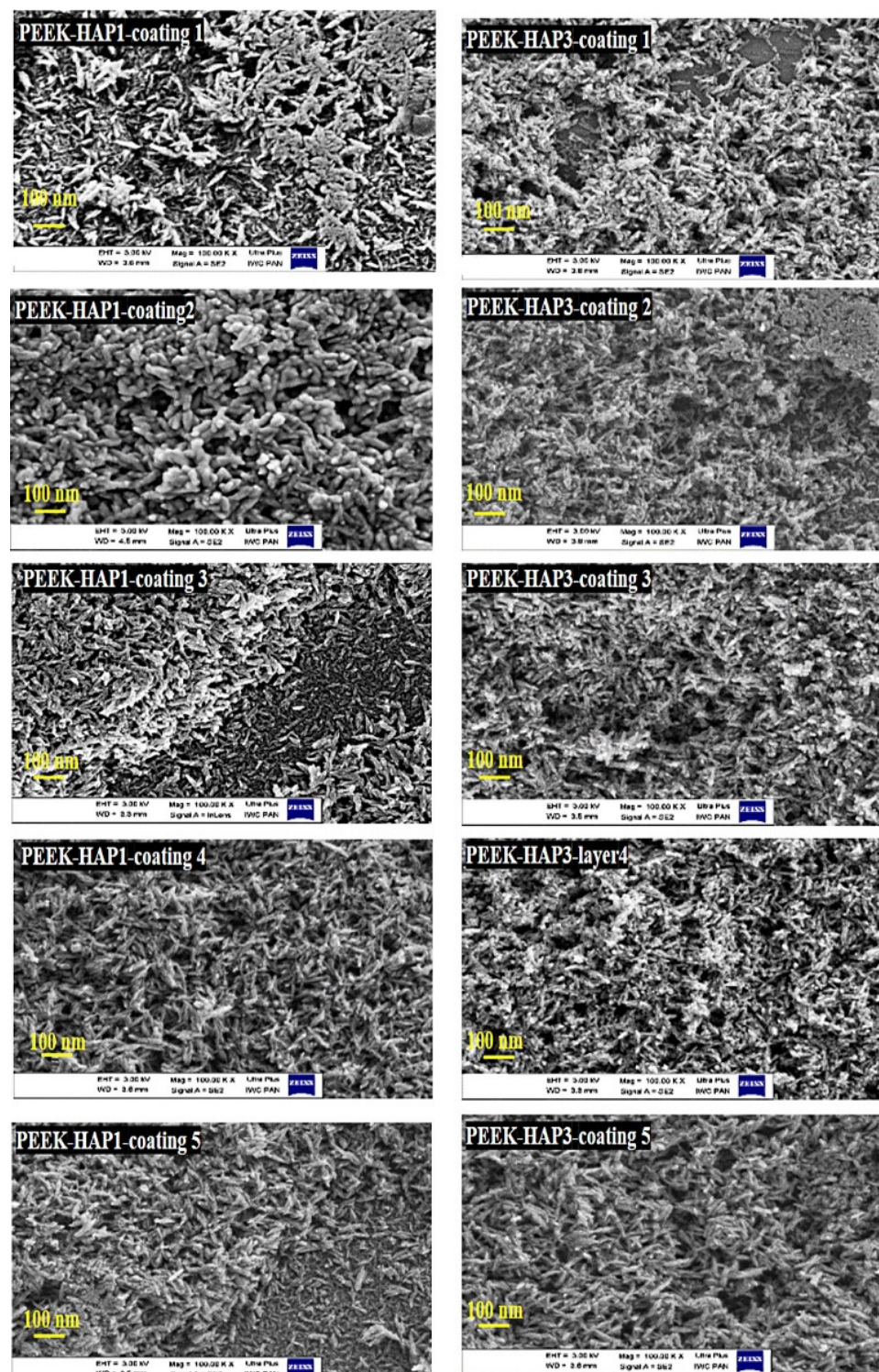


Figure 2. High-magnification FE-SEM images of the morphology of nanoHAP1 and nanoHAP3 after sonocoating PEEK in five subsequent iterations.

Images of fracture-coated PEEK plates are shown in Figure 3. The images of the fractured coatings allowed measurement of the thickness (Table 1). The results illustrate the increase in the GoHAP1 layer thickness with each iteration. The coating was homogeneous, and no cracks were observed. Although the same number of layers was inserted with GoHAP1 and GoHAP3, the layers were proportionally thicker with GoHAP3. This may be due to the bigger grain size of GoHAP3 than GoHAP1.

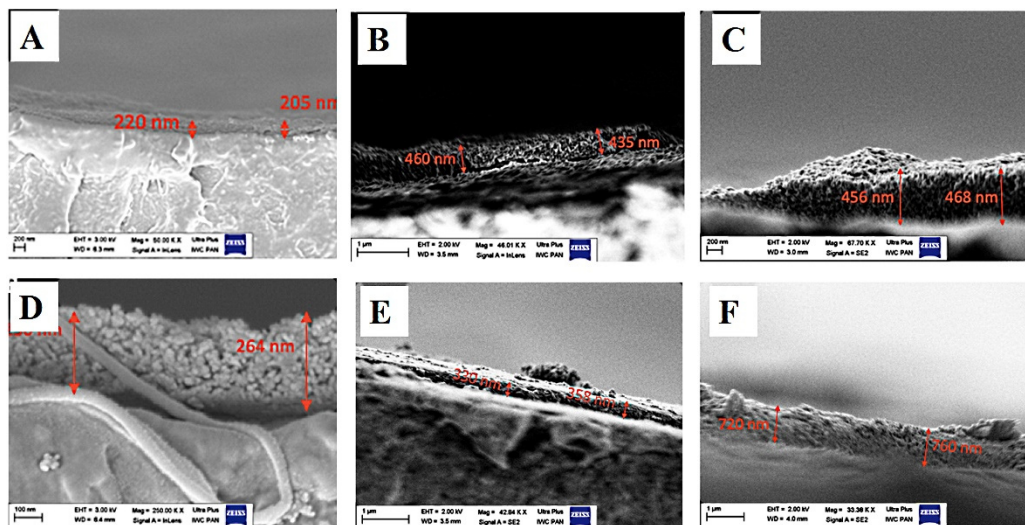


Figure 3. The thickness of layers after sonocoating PEEK substrate with GoHAP1 (A–C) and GoHAP3 (D–F). (A) GoHAP1 for one iteration, (B) three iterations, and (C) five iterations. (D) GoHAP3 for one iteration, (E) two iterations and (F) five iterations.

Table 1. GoHAP coating thickness on a PEEK substrate after several iterations.

	GoHAP1 1st Coating	GoHAP1 2nd Coating	GoHAP1 3rd Coating	GoHAP1 5th Coating
Thickness of layer (nm)	218 ± 33	368 ± 17	462 ± 30	478 ± 20
	GoHAP3 1st Coating	GoHAP3 2nd Coating	GoHAP3 3rd Coating	GoHAP3 5th Coating
Thickness of layer (nm)	246 ± 29	340 ± 40	368 ± 32	763 ± 52

Values are given as mean ± SD.

Most techniques in the literature produce microscale HAP coatings using nano-HAP [18,33,54–56]. These approaches include thermal spraying, plasma exposure, surface modification, spin-coating, cold spraying, aerosol deposition, and sputtering. However, only a few studies have demonstrated the possibility of preparing thin HAP coatings with a thickness in the nano-range. For example, Johansson, et al. produced a thin film layer (20–40 nm) of HAP nanoparticles on PEEK using a deposition technique [21]. This deposited layer seems to not be homogeneous and does not have porosity like the coating obtained by our technique. Therefore, the use of sonochemistry as a green approach for forming bioactive coatings for implants is very promising compared to other traditional techniques, as they are complex processes and require specific conditions, such as high temperature.

The porosity of the coatings is important for drug absorption. The porous structure of the HAP layer influences the bone implant interface, enhancing the ability to encapsulate drugs, induce osteogenic properties, and generate new bone formation [16,57,58]. FE-SEM images (Figure 4) showed that the obtained coatings had different nano-porous structures depending on the iteration of sonocoating. The porosity increased with the number of sonocoating iterations compared to a single layer. The pore size reached 104 ± 34 nm for PEEK-HAP1 and 146 ± 38 nm for PEEK-HAP3 in five iterations. Increased porosity can allow higher drug adsorption.

Overall, the characteristics of the prepared coatings met the requirements for improving drug loading, release and cell regeneration effects [59–62].

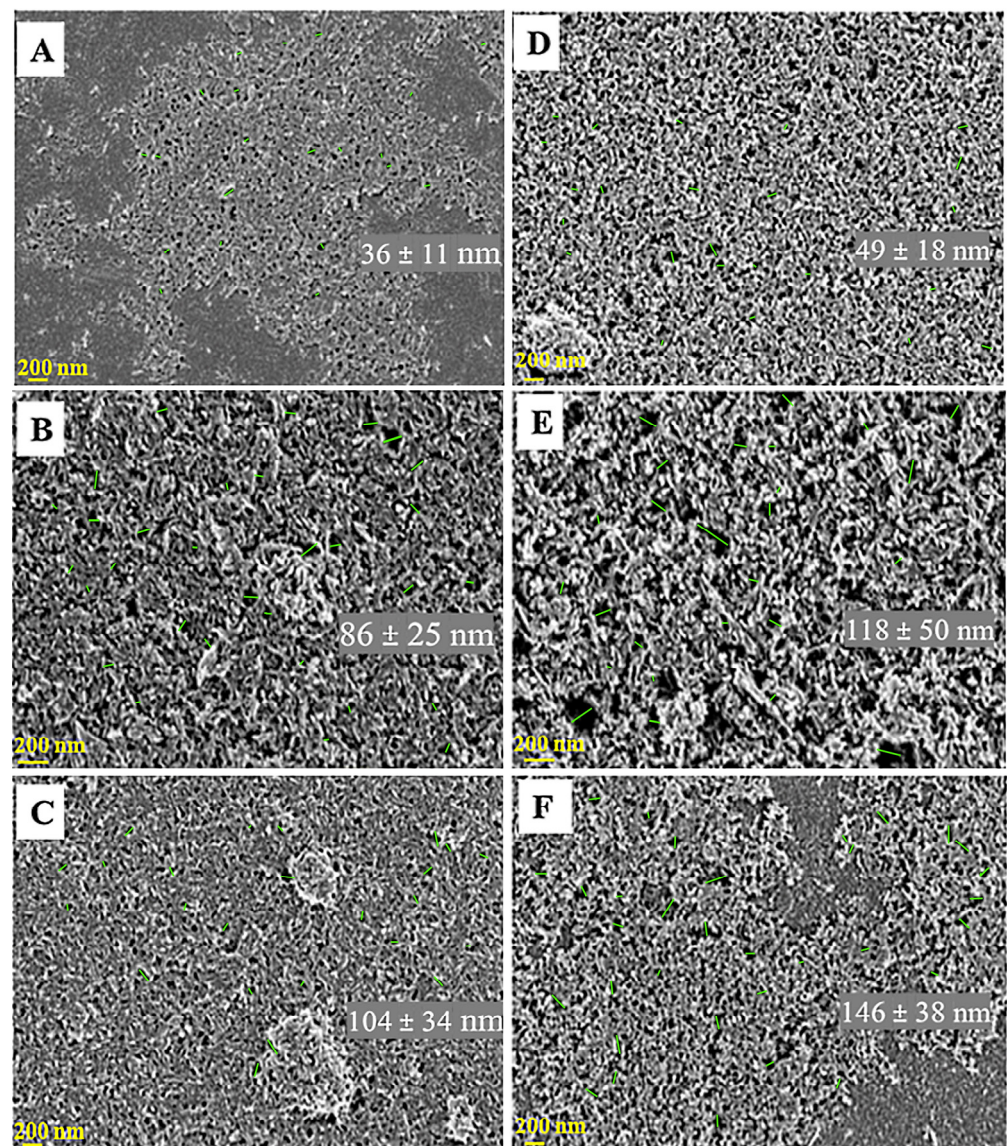


Figure 4. FE-SEM images showing the porosity of the sonocoated PEEK substrate in the nanometer range. (A) GoHAP1 for two iterations, (B) three iterations, and (C) five iterations. (D) GoHAP3 for two iterations, (E) three iterations and (F) five iterations. The green line shows the pore in the coating.

3.2. Contact Angle Measurement of Coatings

Table 2 shows the changes in contact angle before and after PEEK was coated with GoHAP. The GoHAP coatings had a significantly ($p < 0.05$) reduced contact angle with water compared to pristine PEEK ($90^\circ \pm 1^\circ$). These results are in agreement with previous reports [16,63–65]. Comparing all iterations, the lowest contact angle ($55^\circ \pm 2.3^\circ$) was recorded for PEEK-HAP3 coated three times. We also found a significant difference between coating with both GoHAP types. The contact angle was lower when coating with GoHAP3 compared to GoHAP1. The results are important for biomedical applications, as the reduced water contact angle contributes to improved cell attachment, bone growth and bioactivity [66–68].

Table 2. Water contact angle for nanoHAP coating on PEEK substrates after several iterations.

Sample Code	PEEK	HAP1 1st Coating	HAP1 2nd Coating	HAP1 3rd Coating	HAP1 5th Coating	HAP3 1st Coating	HAP3 2nd Coating	HAP3 3rd Coating	HAP3 5th Coating
Contact angle	90° ± 1°	69° ± 4°	69° ± 5°	55° ± 5°	64° ± 4°	52° ± 5°	55° ± 6°	51° ± 5°	54° ± 6°

Values are given as mean ± SD.

3.3. AFM Analysis

We employed AFM for surface imaging because it enables better three-dimensional imaging compared to SEM [69]. Sonocoatings prepared after one iteration of were imaged. Figure 5 shows that the coating on PEEK-GoHAP3 was more homogeneous than PEEK-GoHAP1 after the first coating (Figure 5B,C). Considering the topography of the surface, AFM images of both kinds of coating clearly indicated that the surface is not smooth. We detected that GoHAP nanoparticles formed vertical rod-like shapes (Figure 5D,E). The results are in line with a previous study from Li, et al. on a HAP-coated implant [70]. The topography of the coated surface may influence interfacial cellular functions and cell adhesion, eventually leading to strengthened biological actions between the surface and cells [70,71]. Another reason the sharp rodlike coating on the surface is important, is that it facilitates the interaction with bacterial cells, such as those of *S. aureus* biofilm, and kills them.

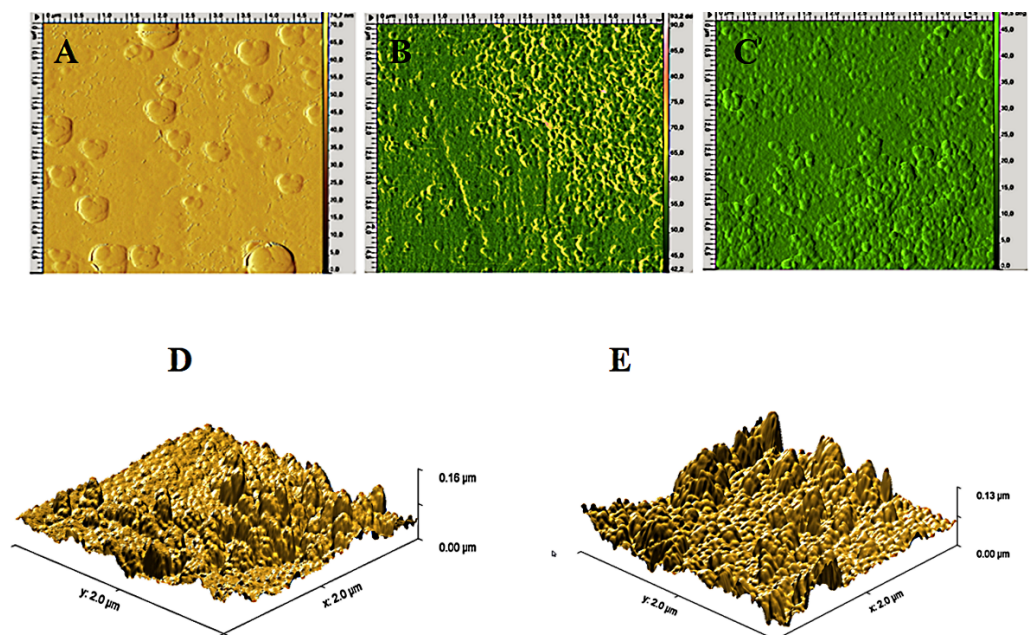


Figure 5. AFM images of uncoated and GoHAP1-coated PEEK after a single iteration. (A) Phase contrast of PEEK, (B) phase contrast of PEEK-GoHAP1, and (C) phase contrast of PEEK-GoHAP3. All are top views. (D) 3D projections of AFM images of PEEK-GoHAP1 and (E) PEEK-GoHAP3.

3.4. FTIR Characterization

The FTIR spectra of PEEK coated with GoHAP and loaded antibiotic are shown in Figure 6. Several peaks appeared for PEEK between 1500 and 500 cm^{-1} , in line with previous studies [29,72]. Further coating with GoHAP resulted in new peaks centered at 1025, 601 and 586 cm^{-1} , corresponding to the nanoHAP powder spectrum. These peaks are associated with the phosphate stretching of P–O at 1025 cm^{-1} and the bending of P–O–P at 601 and 586 cm^{-1} [73,74]. By adding the drug, several peaks corresponding to it can be seen in the PEEK-HAP spectra. In the case of PEEK-HAP1-Cef (Figure 6A), some peaks had increased intensity compared to PEEK-HAP1 (2368, 1755 and 1396 cm^{-1}), whereas many new peaks were detected in the region of 1600 to 500 cm^{-1} , indicating the presence

of the drug. In the case of PEEK-HAP3-Cef (Figure 6B), some peaks had more intense peaks at 2368, 1755, 1396 and 1330 cm^{-1} . A clear difference in the PEEK-HAP3-Cef spectrum compared to PEEK-HAP3, related to the presence of free Cef, was also seen in many regions: the 3500 to 3000 cm^{-1} region centered at $\sim 1600 \text{ cm}^{-1}$, and from approximately 700 to 500 cm^{-1} . Several new peaks corresponding to Cef were also detected, reflecting the successful preparation and loading of Cef onto the nanoHAP coating.

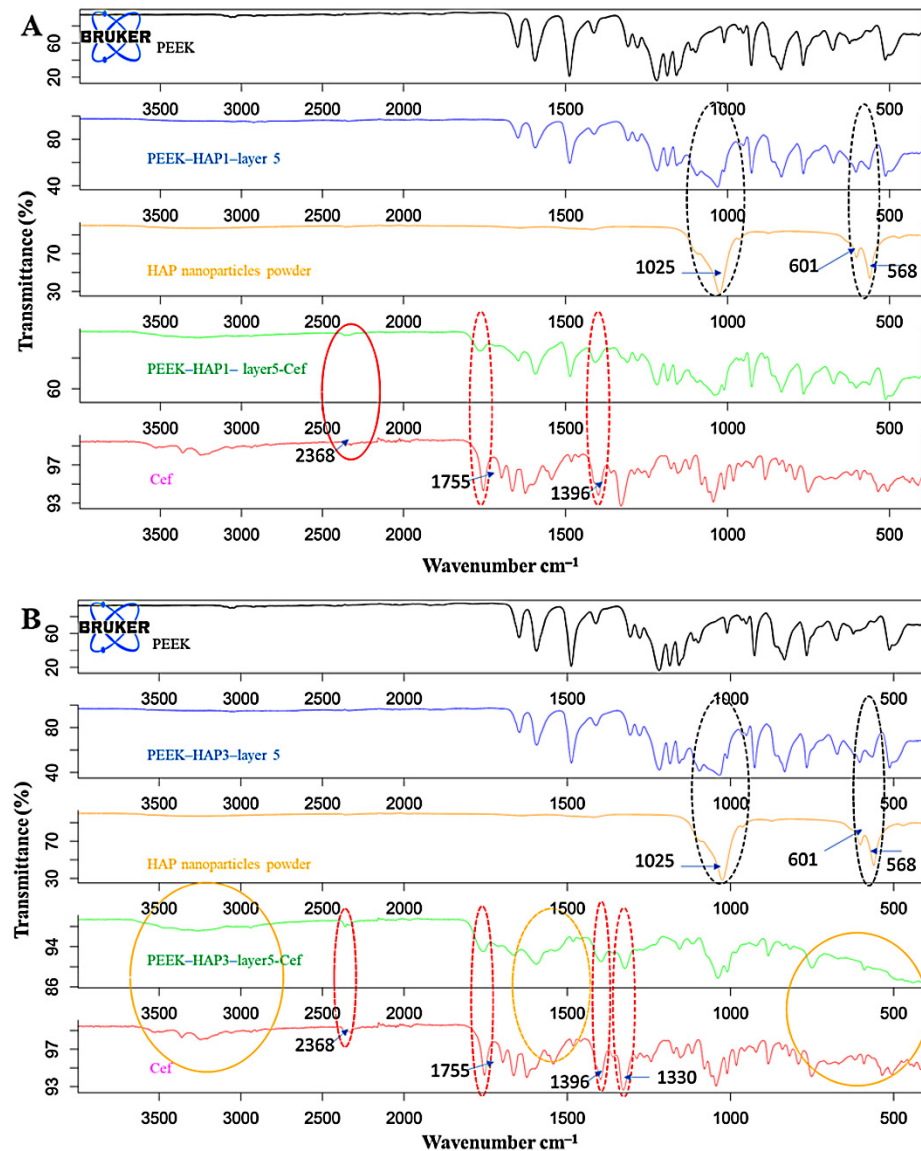


Figure 6. FTIR characterization of uncoated, coated, and Cef-loaded particles after five iterations of sonocoating. (A) GoHAP1, (B) GoHAP3.

3.5. Drug Loading and In Vitro Release

The results of the drug loading experiments are shown in Table 3. We found no significant difference between the amount of drug loaded with the two types of GoHAP. According to previous reports, the amount of drug is sufficient to achieve therapeutic efficacy. For example, Guillot, et al. [75] reported that the loading of bone morphogenetic proteins (BMPs) on PEEK reached $11.3 \pm 0.3 \mu\text{g}/\text{cm}^2$. Another study by Min, et al. [76] on delivering gentamicin formed layer-by-layer reported $7 \mu\text{g}/\text{cm}^2$. Therefore, we hypothesize that such an amount would be sufficient to prevent biofilm formation.

Table 3. Amount of Cef loaded in GoHAP-coated PEEK after five iterations.

GoHAP Type	Mean Drug \pm SD (mg/Substrate 1 cm ²)
PEEK-GoHAP1-Cef	1.09 \pm 0.13
PEEK-GoHAP3-Cef	0.94 \pm 0.16

No significant differences were found by means of least significance differences from one-way ANOVA.

The in vitro release profiles of Cef from GoHAP-coated PEEK are shown in Figure 7. There was a substantial initial “burst” release with nearly 96% of the drug being released in the first 24 h. The rapid release of Cef could be attributed to drug molecules attached to the surface having weak bonds and the high amount to the high porosity of the layer. A similar effect was observed for Cef released from PEEK coated with GoHAP3 but with a different release percentage (Figure 7B). Approximately 80%, 86% and 86.1% of the total amount of Cef was released within 2 h, 6.5 h and 24 h, respectively, followed by the release of approximately 86% up to 100 h, increasing to ~89% at 150 h. The quick release of Cef within 24 h accompanied by a linear effect up to 150 h is promising for the treatment of surgical site infection because *S. aureus* is able to produce biofilm between 24 and 72 h [5]. Therefore, such a release profile would be efficient to prevent attachment of the microbes. In contrast to cefuroxime release studies [77–80], no study has related the release profile of Cef sodium salt from nanoHAP or medical implants. The usage of Cef in sodium salt form by means of a local delivery system [46] is needed because the salt form is effective but not chemically stable [43].

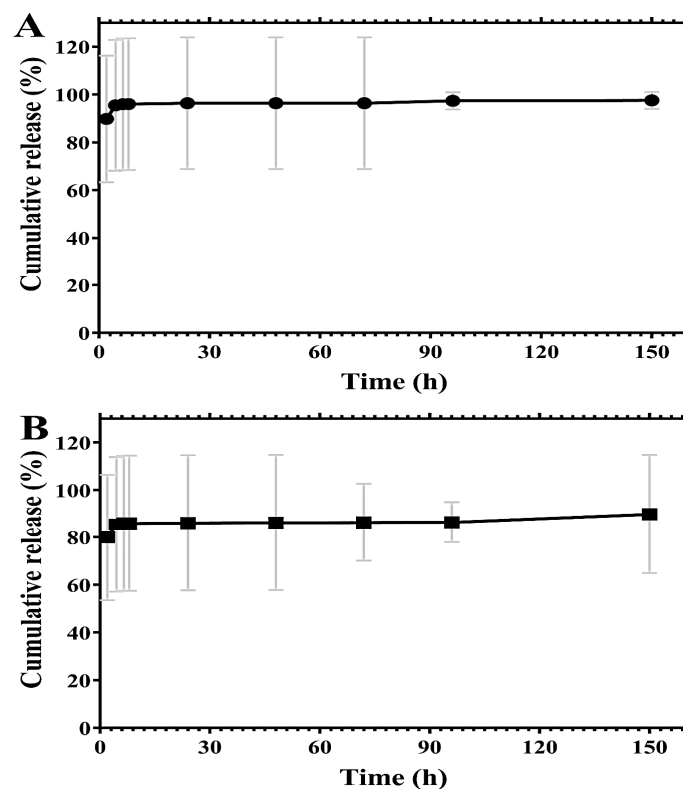


Figure 7. (A) In vitro release of Cef from PEEK-GoHAP1-Cef (B) and PEEK-GoHAP3-Cef in PBS release medium. Data are presented as mean \pm SD.

3.6. Antibacterial Evaluations

We used two different methods to evaluate the killing efficiency of the drug-infiltrated coatings against *S. aureus*. Figure 8 discloses the effective killing of *S. aureus* when grown on PEEK-HAP1-Cef compared to PEEK and PEEK-HAP1 in the inhibition zone test. The average inhibition zone diameter after 24 h was 45.0 mm \pm 2.0 mm, which is considered a

wide inhibition zone for the cultured bacteria. We observed that the zones were the same after 5 days of incubation and 11 days of incubation. These results are in line with previous studies on antibiotic coatings against *S. aureus* and other bacteria [17,18,81].



Figure 8. The antibacterial activity against *Staphylococcus aureus* by means of zone inhibition after incubation for 24 h with PEEK-GoHAP1 and PEEK-GoHAP1-Cef compared to control.

When examining the antibacterial effect by means of the broth dilution method, the PEEK-HAP1-Cef sample possessed a higher antibacterial effect against *S. aureus* compared to PEEK-HAP1 and the control sample (PEEK only; Figure 9A). The OD recorded for PEEK-HAP1-Cef was close to zero with linear performance over 168 h, whereas a high OD was detected for PEEK-HAP1 and control. The efficient killing of bacteria over 168 h is probably related to the amount of drug loaded ($\sim 1 \text{ mg/cm}^2$) and the release effect with an initial burst effect followed by a stable release up to 150 h. These results indicate that PEEK with a GoHAP layer loaded with Cef prevents *S. aureus* over a long period of time (i.e., 168 h), which is required for antibacterial implants. There seems to be a good relationship between the loaded amount, release effect, and antibacterial activity. Photos of the tested tubes are presented in Figure 9B, showing that the presence of Cef led to a clear picture (no observed bacterial growth) compared to PEEK-HAP1 and control samples. This observation confirms the results obtained with the broth dilution method.

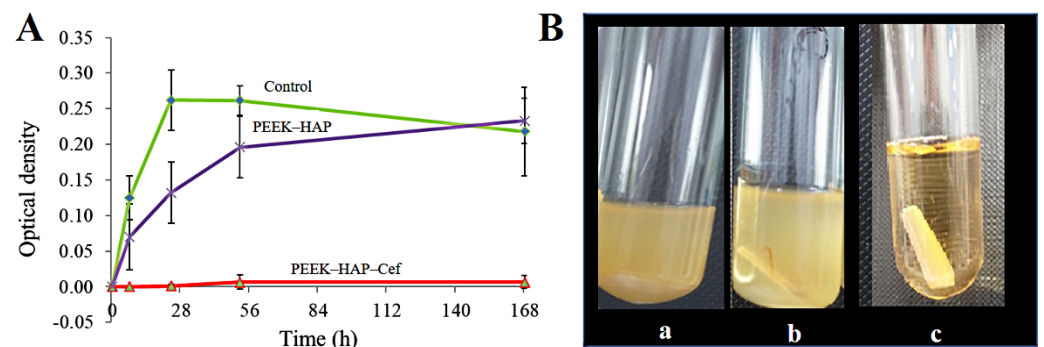


Figure 9. (A) The antibacterial activity against *Staphylococcus aureus* ATCC 25923 by means of the broth dilution method with PEEK-GoHAP1 and PEEK-GoHAP1-Cef compared to control. Data are presented as mean \pm SD. (B) Photograph of the tubes after experiments: control (a), PEEK-GoHAP1 (b) and PEEK-GoHAP1-Cef (c).

For further evaluation of the antibacterial properties, we used the broth dilution method to change the broth from the samples and supply a new volume of broth. Removing the broth should remove the drug because it is a water-soluble compound. For this reason, we changed the broth two times after incubation for 10 and 24.5 h (Figure 10). PEEK-HAP1-Cef had a lower OD compared to the control. By changing the broth at 10 h and 24.5 h, the OD increased, especially at 25.5 h compared to 10 h, compared to the OD before

changing the broth. Interestingly, these results disclose that Cef is attached to the surface as well as in the pores of GoHAP.

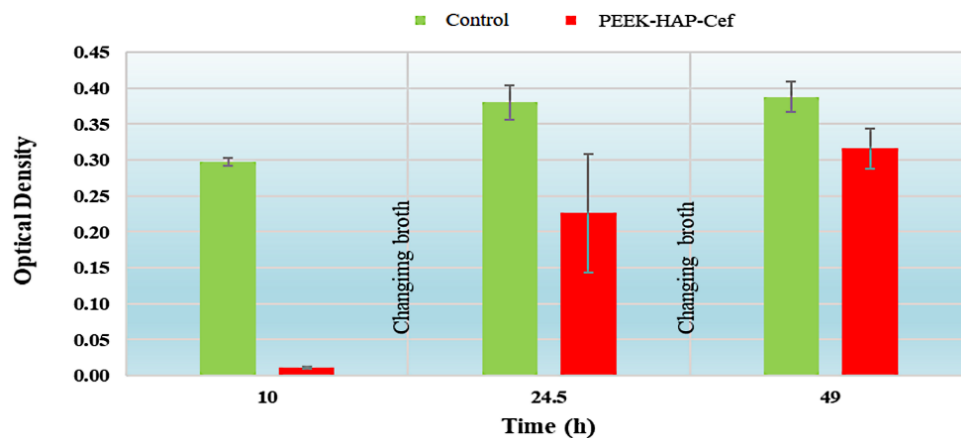


Figure 10. The antibacterial activity against *Staphylococcus aureus* ATCC 25923 by means of the broth dilution method (with change of broth medium) after incubation of up to 49 PEEK-GoHAP1-Cef compared to control. Data are presented as mean \pm SD.

Overall, the results obtained in antibacterial evaluation studies have demonstrated that PEEK-HAP-Cef coatings not only facilitate a short-term antibacterial effect, but also promote protection from *S. aureus*. Bone growth could be promoted because a small fraction of drug is present in the GoHAP layer and more on the surface. Our results are in line with earlier studies highlighting the importance of the antibacterial effects of HAP coatings [17,82–84].

Coating medical implants with HAP nanoparticles using sonocoating has many advantages. This fabrication method does not affect the structure and crystallinity of the nanoHAP because the coating temperature is low. The same factor is responsible for the layer possessing a highly active surface and nanoporosity, allowing a relatively large amount of drug to be loaded per unit area.

4. Conclusions

The sonocoating technique achieves a layer of nano-hydroxyapatite GoHAP on the surface of PEEK via a facile process. The technique allows the thickness to be controlled in the range of 200 to 760 nm. The sonocoated material is strongly hydrophilic. The GoHAP layer has a highly developed specific surface that favors drug absorption. Absorption of Cef antibiotics of up to 1 mg/cm² was achieved. The amount of drug loaded can be controlled by the type of GoHAP, the thickness and porosity of the layer, and the concentration of the drug. An initial burst of 86 to 96% of the drug being released within 24 h is followed by a linear, stable release. The PEEK-HAP1-Cef coating has a sufficient antibacterial effect against *S. aureus*, as shown by zone inhibition and broth dilution. Thus, our results could pave the way for antibacterial coatings on medical implants.

Author Contributions: Conceptualization, K.A., W.L. and E.P.; methodology, K.A., M.B. and J.N.; formal analysis, K.A., M.B., D.F., B.W., A.S.-S. and M.L.; investigation, K.A., M.B., D.F., U.S. and J.N.; resources, W.L., W.S. and B.S.; original draft preparation, K.A.; revision, K.A., W.L., E.P., A.S.-S., M.B., B.S. and W.S.; supervision, W.L. All authors have read and agreed to the published version of the manuscript.

Funding: Funding was received from the National Center for Research and Development, Poland (STRATEGMED3/306888/3/NCBR/2017, project iTE). We also thank the Ministry of Education and Science for the subsidy funds. The research was carried out using equipment funded by the CePT project (reference no. POIG.02.02.00-14-024/08), which is financed by the European Regional Development Fund within the Operational Programme “Innovative Economy” for 2007–2013.

Acknowledgments: The authors would like to thank Adam Presz, and Jan Mizeracki from the Laboratory of Nanostructures and Nanomedicine, Institute of High Pressure Physics, Polish Academy of Sciences, for the FE-SEM analysis.

Conflicts of Interest: The authors declare no conflict of interest.

References

1. Gunpath, U.; Le, H. 6—Composite coatings for implants and tissue engineering scaffolds. In *Biomedical Composites*, 2nd ed.; Ambrosio, L., Ed.; Woodhead Publishing: Sawston, UK, 2017; pp. 111–138.
2. Wang, M.; Tang, T. Surface treatment strategies to combat implant-related infection from the beginning. *J. Orthop. Transl.* **2019**, *17*, 42–54. [[CrossRef](#)]
3. Mangram, A.J.; Horan, T.C.; Pearson, M.L.; Silver, L.C.; Jarvis, W.R.; Hospital Infection Control Practices Advisory Committee. Guideline for prevention of surgical site infection. *Infect. Control Hosp. Epidemiol.* **1999**, *20*, 250–278. [[CrossRef](#)] [[PubMed](#)]
4. Darouiche, R.O. Treatment of Infections Associated with Surgical Implants. *N. Engl. J. Med.* **2004**, *350*, 1422–1429. [[CrossRef](#)] [[PubMed](#)]
5. Oliveira, M.; Nunes, S.F.; Carneiro, C.; Bexiga, R.; Bernardo, F.; Vilela, C.L. Time course of biofilm formation by *Staphylococcus aureus* and *Staphylococcus epidermidis* mastitis isolates. *Vet. Microbiol.* **2007**, *124*, 187–191. [[CrossRef](#)] [[PubMed](#)]
6. Zilberman, M.; Elsner, J.J. Antibiotic-eluting medical devices for various applications. *J. Control. Release* **2008**, *130*, 202–215. [[CrossRef](#)] [[PubMed](#)]
7. Bazaka, K.; Jacob, M.V.; Crawford, R.J.; Ivanova, E.P. Efficient surface modification of biomaterial to prevent biofilm formation and the attachment of microorganisms. *Appl. Microbiol. Biotechnol.* **2012**, *95*, 299–311. [[CrossRef](#)] [[PubMed](#)]
8. Boase, N.R.B.; Torres, M.D.T.; Fletcher, N.L.; de la Fuente-Nunez, C.; Fairfull-Smith, K.E. Polynitroxide copolymers to reduce biofilm fouling on surfaces. *Polym. Chem.* **2018**, *9*, 5308–5318. [[CrossRef](#)]
9. Guilhen, C.; Forestier, C.; Balestrino, D. Biofilm dispersal: Multiple elaborate strategies for dissemination of bacteria with unique properties. *Mol. Microbiol.* **2017**, *105*, 188–210. [[CrossRef](#)]
10. Narayana, S.V.V.S.P.; Srihari, S.V.V.P. A Review on Surface Modifications and Coatings on Implants to Prevent Biofilm. *Regen. Eng. Transl. Med.* **2019**. [[CrossRef](#)]
11. Bruellhoff, K.; Fiedler, J.; Möller, M.; Groll, J.; Brenner, R.E. Surface Coating Strategies to Prevent Biofilm Formation on Implant Surfaces. *Int. J. Artif. Organs* **2010**, *33*, 646–653. [[CrossRef](#)]
12. Cloutier, M.; Mantovani, D.; Rosei, F. Antibacterial Coatings: Challenges, Perspectives, and Opportunities. *Trends Biotechnol.* **2015**, *33*, 637–652. [[CrossRef](#)]
13. Pan, C.; Zhou, Z.; Yu, X. Coatings as the useful drug delivery system for the prevention of implant-related infections. *J. Orthop. Surg. Res.* **2018**, *13*, 220. [[CrossRef](#)]
14. Higuchi, J.; Fortunato, G.; Wozniak, B.; Chodara, A.; Domaschke, S.; Meczynska-Wielgosz, S.; Kruszewski, M.; Dommann, A.; Lojkowski, W. Polymer Membranes Sono-coated and Electro-sprayed with Nano-Hydroxyapatite for Periodontal Tissues Regeneration. *Nanomaterials* **2019**, *9*, 1625. [[CrossRef](#)]
15. Smolen, D.; Chudoba, T.; Malka, I.; Kedzierska, A.; Lojkowski, W.; Swieszkowski, W.; Kurzydowski, K.J.; Kolodziejczyk-Mierzynska, M.; Lewandowska-Szumiel, M. Highly biocompatible, nanocrystalline hydroxyapatite synthesized in a solvothermal process driven by high energy density microwave radiation. *Int. J. Nanomed.* **2013**, *8*, 653–668. [[CrossRef](#)]
16. Rogowska-Tylman, J.; Locs, J.; Salma, I.; Woźniak, B.; Pilmane, M.; Zalite, V.; Wojnarowicz, J.; Kędzierska-Sar, A.; Chudoba, T.; Szlajak, K.; et al. In vivo and in vitro study of a novel nanohydroxyapatite sono-coated scaffolds for enhanced bone regeneration. *Mater. Sci. Eng. C* **2019**, *99*, 669–684. [[CrossRef](#)] [[PubMed](#)]
17. Stigter, M.; Bezemer, J.; de Groot, K.; Layrolle, P. Incorporation of different antibiotics into carbonated hydroxyapatite coatings on titanium implants, release and antibiotic efficacy. *J. Control. Release* **2004**, *99*, 127–137. [[CrossRef](#)] [[PubMed](#)]
18. Geuli, O.; Metoki, N.; Zada, T.; Reches, M.; Eliaz, N.; Mandler, D. Synthesis, coating, and drug-release of hydroxyapatite nanoparticles loaded with antibiotics. *J. Mater. Chem. B* **2017**, *5*, 7819–7830. [[CrossRef](#)]
19. Huang, D.; Zuo, Y.; Zou, Q.; Zhang, L.; Li, J.; Cheng, L.; Shen, J.; Li, Y. Antibacterial Chitosan Coating on Nano-hydroxyapatite/Polyamide66 Porous Bone Scaffold for Drug Delivery. *J. Biomater. Sci. Polym. Ed.* **2011**, *22*, 931–944. [[CrossRef](#)] [[PubMed](#)]
20. Prasanna, A.P.S.; Venkatasubbu, G.D. Sustained release of amoxicillin from hydroxyapatite nanocomposite for bone infections. *Prog. Biomater.* **2018**, *7*, 289–296. [[CrossRef](#)]
21. Johansson, P.; Jimbo, R.; Kozai, Y.; Sakurai, T.; Kjellin, P.; Currie, F.; Wennerberg, A. Nanosized Hydroxyapatite Coating on PEEK Implants Enhances Early Bone Formation: A Histological and Three-Dimensional Investigation in Rabbit Bone. *Materials* **2015**, *8*, 3815–3830. [[CrossRef](#)]
22. Campbell, A.A.; Song, L.; Li, X.S.; Nelson, B.J.; Bottoni, C.; Brooks, D.E.; DeJong, E.S. Development, characterization, and antimicrobial efficacy of hydroxyapatite-chlorhexidine coatings produced by surface-induced mineralization. *J. Biomed. Mater. Res.* **2000**, *53*, 400–407. [[CrossRef](#)]
23. Szałaj, U.; Świdarska-Środa, A.; Chodara, A.; Gierlotka, S.; Łojkowski, W. Nanoparticle Size Effect on Water Vapour Adsorption by Hydroxyapatite. *Nanomaterials* **2019**, *9*, 1005. [[CrossRef](#)] [[PubMed](#)]

24. Tian, B.; Tang, S.; Wang, C.D.; Wang, W.G.; Wu, C.L.; Guo, Y.J.; Guo, Y.P.; Zhu, Z.A. Bactericidal properties and biocompatibility of a gentamicin-loaded Fe₃O₄/carbonated hydroxyapatite coating. *Colloids Surf. B Biointerfaces* **2014**, *123*, 403–412. [[CrossRef](#)] [[PubMed](#)]
25. Kolmas, J.; Groszyk, E.; Kwiatkowska-Różycka, D. Substituted Hydroxyapatites with Antibacterial Properties. *Biomed. Res. Int.* **2014**, *2014*, 178123. [[CrossRef](#)] [[PubMed](#)]
26. Pan, J.; Prabakaran, S.; Rajan, M. In-vivo assessment of minerals substituted hydroxyapatite/poly sorbitol sebacate glutamate (PSSG) composite coating on titanium metal implant for orthopedic implantation. *Biomed. Pharmacother.* **2019**, *119*, 109404. [[CrossRef](#)] [[PubMed](#)]
27. Kurtz, S.M.; Devine, J.N. PEEK biomaterials in trauma, orthopedic, and spinal implants. *Biomaterials* **2007**, *28*, 4845–4869. [[CrossRef](#)]
28. Rabiei, A.; Sandukas, S. Processing and evaluation of bioactive coatings on polymeric implants. *J. Biomed. Mater. Res. A* **2013**, *101*, 2621–2629. [[CrossRef](#)]
29. Baştan, F.E.; Rehman, M.A.U.; Avcu, Y.Y.; Avcu, E.; Üstel, F.; Boccaccini, A.R. Electrophoretic co-deposition of PEEK-hydroxyapatite composite coatings for biomedical applications. *Colloids Surf. B Biointerfaces* **2018**, *169*, 176–182. [[CrossRef](#)]
30. Masamoto, K.; Fujibayashi, S.; Yabutsuka, T.; Hiruta, T.; Otsuki, B.; Okuzu, Y.; Goto, K.; Shimizu, T.; Shimizu, Y.; Ishizaki, C.; et al. In vivo and in vitro bioactivity of a “precursor of apatite” treatment on polyetheretherketone. *Acta Biomater.* **2019**, *91*, 48–59. [[CrossRef](#)]
31. Zhu, C.; He, M.; Mao, L.; Li, T.; Zhang, L.; Liu, L.; Feng, G.; Song, Y. Titanium-interlayer mediated hydroxyapatite coating on polyetheretherketone: A prospective study in patients with single-level cervical degenerative disc disease. *J. Transl. Med.* **2021**, *19*, 14. [[CrossRef](#)]
32. Townsend, L.; Williams, R.L.; Anuforum, O.; Berwick, M.R.; Halstead, F.; Hughes, E.; Stamboulis, A.; Oppenheim, B.; Gough, J.; Grover, L.; et al. Antimicrobial peptide coatings for hydroxyapatite: Electrostatic and covalent attachment of antimicrobial peptides to surfaces. *J. R. Soc. Interface* **2017**, *14*. [[CrossRef](#)] [[PubMed](#)]
33. Yang, C.-C.; Lin, C.-C.; Liao, J.-W.; Yen, S.-K. Vancomycin–chitosan composite deposited on post porous hydroxyapatite coated Ti6Al4V implant for drug controlled release. *Mater. Sci. Eng. C* **2013**, *33*, 2203–2212. [[CrossRef](#)]
34. Forsgren, J.; Brohede, U.; Mihranyan, A.; Engqvist, H.; Strömme, M. Fast loading, slow release—a new strategy for incorporating antibiotics to hydroxyapatite. In *Proceedings of the Key Engineering Materials*; Trans Tech Publications Ltd.: Bäch SZ, Switzerland, 2009; pp. 523–526.
35. Hussain, S.; Rutledge, L.; Acheson, J.G.; Meenan, B.J.; Boyd, A.R. The Surface Characterisation of Polyetheretherketone (PEEK) Modified via the Direct Sputter Deposition of Calcium Phosphate Thin Films. *Coatings* **2020**, *10*, 1088. [[CrossRef](#)]
36. Duta, L.; Neamtu, J.; Melinte, R.P.; Zureigat, O.A.; Popescu-Pelin, G.; Chioibas, D.; Oktar, F.N.; Popescu, A.C. In Vivo Assessment of Bone Enhancement in the Case of 3D-Printed Implants Functionalized with Lithium-Doped Biological-Derived Hydroxyapatite Coatings: A Preliminary Study on Rabbits. *Coatings* **2020**, *10*, 992. [[CrossRef](#)]
37. Wrona, A.; Bilewska, K.; Lis, M.; Kamińska, M.; Olszewski, T.; Pajzderski, P.; Więclaw, G.; Jaśkiewicz, M.; Kamysz, W. Antimicrobial properties of protective coatings produced by plasma spraying technique. *Surf. Coat. Technol.* **2017**, *318*, 332–340. [[CrossRef](#)]
38. Beddow, J.; Singh, G.; Blanes, M.; Molla, K.; Perelshtein, I.; Gedanken, A.; Joyce, E.; Mason, T. Sonochemical coating of textile fabrics with antibacterial nanoparticles. *AIP Conf. Proc.* **2012**, *1433*, 400–403. [[CrossRef](#)]
39. Perelshtein, I.; Lipovsky, A.; Perkas, N.; Tzanov, T.; Gedanken, A. Sonochemical co-deposition of antibacterial nanoparticles and dyes on textiles. *Beilstein J. Nanotechnol.* **2016**, *7*, 1–8. [[CrossRef](#)]
40. Svirinovsky, A.; Perelshtein, I.; Natan, M.; Banin, E.; Gedanken, A. Imparting superhydrophobic and biocidal functionalities to a polymeric substrate by the sonochemical method. *Ultrason. Sonochem.* **2018**, *44*, 398–403. [[CrossRef](#)]
41. Golda-Cepa, M.; Chytrosz, P.; Chorylek, A.; Kotarba, A. One-step sonochemical fabrication and embedding of gentamicin nanoparticles into parylene C implant coating: Towards controlled drug delivery. *Nanomed. Nanotechnol. Biol. Med.* **2018**, *14*, 941–950. [[CrossRef](#)] [[PubMed](#)]
42. Woźniak, B.; Szałaj, U.; Chodara, A.; Mizeracki, J.; Łojkowski, M.; Myszka, D.; Łojkowski, W. Mechanism for sonocoating a polymer surface with nano-hydroxyapatite. *Mater. Lett.* **2019**, *249*, 155–159. [[CrossRef](#)]
43. Liu, W.J.; Ma, C.Y.; Feng, S.X.; Wang, X.Z. Solubility Measurement and Stability Study of Sodium Cefuroxime. *J. Chem. Eng. Data* **2014**, *59*, 807–816. [[CrossRef](#)]
44. Greenwood, D.; Pearson, N.J.; O’Grady, F. Cefuroxime: A new cephalosporin antibiotic with enhanced stability to enterobacterial β -lactamases. *J. Antimicrob. Chemother.* **1976**, *2*, 337–343. [[CrossRef](#)]
45. Zhao, L.; Li, Q.; Li, X.; Yin, R.; Chen, X.; Geng, L.; Bi, K. Bioequivalence and population pharmacokinetic modeling of two forms of antibiotic, cefuroxime lysine and cefuroxime sodium, after intravenous infusion in beagle dogs. *J. Biomed. Biotechnol.* **2012**, *2012*, 507294. [[CrossRef](#)] [[PubMed](#)]
46. Racovita, S.; Lungan, M.A.; Bunia, I.; Popa, M.; Vasiliu, S. Adsorption and release studies of cefuroxime sodium from acrylic ion exchange resin microparticles coated with gellan. *React. Funct. Polym.* **2016**, *105*, 103–113. [[CrossRef](#)]
47. Gold, B.; Rodriguez, W.J. Cefuroxime: Mechanisms of action, antimicrobial activity, pharmacokinetics, clinical applications, adverse reactions and therapeutic indications. *Pharmacotherapy* **1983**, *3*, 82–100. [[CrossRef](#)]
48. Salzmann, G.M.; Naal, F.D.; von Knoch, F.; Tuebel, J.; Gradinger, R.; Imhoff, A.B.; Schauwecker, J. Effects of cefuroxime on human osteoblasts in vitro. *J. Biomed. Mater. Res. A* **2007**, *82*, 462–468. [[CrossRef](#)]

49. Lovering, A.M.; Perez, J.; Bowker, K.E.; Reeves, D.S.; MacGowan, A.P.; Bannister, G. A comparison of the penetration of cefuroxime and cephamandole into bone, fat and haematoma fluid in patients undergoing total hip replacement. *J. Antimicrob. Chemother.* **1997**, *40*, 99–104. [[CrossRef](#)] [[PubMed](#)]
50. McQueen, M.M.; Hughes, S.P.F.; May, P.; Verity, L. Cefuroxime in total joint arthroplasty: Intravenous or in bone cement. *J. Arthroplast.* **1990**, *5*, 169–172. [[CrossRef](#)]
51. Kuśnieruk, S.; Wojnarowicz, J.; Chodara, A.; Chudoba, T.; Gierlotka, S.; Lojkowski, W. Influence of hydrothermal synthesis parameters on the properties of hydroxyapatite nanoparticles. *Beilstein J. Nanotechnol.* **2016**, *7*, 1586–1601. [[CrossRef](#)]
52. Andrzej, M.; Jan, W.; Jan, P.; Tadeusz, C.; Jacek, W. A Novel Reactor for Microwave Hydrothermal Scale-up Nanopowder Synthesis. *Int. J. Chem. React. Eng.* **2013**, *11*, 361–368. [[CrossRef](#)]
53. Assaad, H.I.; Zhou, L.; Carroll, R.J.; Wu, G. Rapid publication-ready MS-Word tables for one-way ANOVA. *Springerplus* **2014**, *3*, 474. [[CrossRef](#)]
54. Dorozhkin, S.V. Calcium orthophosphate coatings, films and layers. *Prog. Biomater.* **2012**, *1*, 1–40. [[CrossRef](#)]
55. Wang, B.C.; Lee, T.M.; Chang, E.; Yang, C.Y. The shear strength and the failure mode of plasma-sprayed hydroxyapatite coating to bone: The effect of coating thickness. *J. Biomed. Mater. Res.* **1993**, *27*, 1315–1327. [[CrossRef](#)] [[PubMed](#)]
56. Tian, Q.; Lin, J.; Rivera-Castaneda, L.; Tسانhani, A.; Dunn, Z.S.; Rodriguez, A.; Aslani, A.; Liu, H. Nano-to-Submicron Hydroxyapatite Coatings for Magnesium-based Bioresorbable Implants—Deposition, Characterization, Degradation, Mechanical Properties, and Cytocompatibility. *Sci. Rep.* **2019**, *9*, 810. [[CrossRef](#)]
57. Jing, W.; Zhang, M.; Jin, L.; Zhao, J.; Gao, Q.; Ren, M.; Fan, Q. Assessment of osteoinduction using a porous hydroxyapatite coating prepared by micro-arc oxidation on a new titanium alloy. *Int. J. Surg.* **2015**, *24*, 51–56. [[CrossRef](#)] [[PubMed](#)]
58. Son, J.S.; Choi, Y.-A.; Park, E.-K.; Kwon, T.-Y.; Kim, K.-H.; Lee, K.-B. Drug delivery from hydroxyapatite-coated titanium surfaces using biodegradable particle carriers. *J. Biomed. Mater. Res. Part B Appl. Biomater.* **2013**, *101*, 247–257. [[CrossRef](#)] [[PubMed](#)]
59. Wang, L.; Huang, F.; Wu, Z.; Ma, R. Biocompatibility of nano-hydroxyapatite/polyetheretherketone composite materials with osteoblasts cultured in vitro. *AIP Conf. Proc.* **2017**, *1829*, 020004. [[CrossRef](#)]
60. Shuai, C.; Shuai, C.; Wu, P.; Yuan, F.; Feng, P.; Yang, Y.; Guo, W.; Fan, X.; Su, T.; Peng, S.; et al. Characterization and Bioactivity Evaluation of (Polyetheretherketone/Polyglycolicacid)-Hydroxyapatite Scaffolds for Tissue Regeneration. *Materials* **2016**, *9*, 934. [[CrossRef](#)]
61. Murphy, C.M.; Haugh, M.G.; O'Brien, F.J. The effect of mean pore size on cell attachment, proliferation and migration in collagen-glycosaminoglycan scaffolds for bone tissue engineering. *Biomaterials* **2010**, *31*, 461–466. [[CrossRef](#)]
62. Walsh, W.R.; Pelletier, M.H.; Bertollo, N.; Christou, C.; Tan, C. Does PEEK/HA Enhance Bone Formation Compared with PEEK in a Sheep Cervical Fusion Model? *Clin. Orthop. Relat. Res.* **2016**, *474*, 2364–2372. [[CrossRef](#)]
63. Tahmasbi Rad, A.; Solati-Hashjin, M.; Osman, N.A.A.; Faghihi, S. Improved bio-physical performance of hydroxyapatite coatings obtained by electrophoretic deposition at dynamic voltage. *Ceram. Int.* **2014**, *40*, 12681–12691. [[CrossRef](#)]
64. Jung, U.-W.; Hwang, J.-W.; Choi, D.-Y.; Hu, K.-S.; Kwon, M.-K.; Choi, S.-H.; Kim, H.-J. Surface characteristics of a novel hydroxyapatite-coated dental implant. *J. Periodontal Implant Sci.* **2012**, *42*, 59–63. [[CrossRef](#)] [[PubMed](#)]
65. Almasi, D.; Lau, W.J.; Rasae, S.; Sharifi, R.; Mozaffari, H.R. Fabrication of a novel hydroxyapatite/polyether ether ketone surface nanocomposite via friction stir processing for orthopedic and dental applications. *Prog. Biomater.* **2020**, *9*, 35–44. [[CrossRef](#)] [[PubMed](#)]
66. Eliaz, N.; Shmueli, S.; Shur, I.; Benayahu, D.; Aronov, D.; Rosenman, G. The effect of surface treatment on the surface texture and contact angle of electrochemically deposited hydroxyapatite coating and on its interaction with bone-forming cells. *Acta Biomater.* **2009**, *5*, 3178–3191. [[CrossRef](#)]
67. Yu, H.-N.; Hsu, H.-C.; Wu, S.-C.; Hsu, C.-W.; Hsu, S.-K.; Ho, W.-F. Characterization of Nano-Scale Hydroxyapatite Coating Synthesized from Eggshells Through Hydrothermal Reaction on Commercially Pure Titanium. *Coatings* **2020**, *10*, 112. [[CrossRef](#)]
68. Zhao, B.; Li, X.; Xu, H.; Jiang, Y.; Wang, D.; Liu, R. Influence of Simvastatin-Strontium-Hydroxyapatite Coated Implant Formed by Micro-Arc Oxidation and Immersion Method on Osteointegration in Osteoporotic Rabbits. *Int. J. Nanomed.* **2020**, *15*, 1797–1807. [[CrossRef](#)] [[PubMed](#)]
69. Cometa, S.; Bonifacio, M.A.; Ferreira, A.M.; Gentile, P.; De Giglio, E. Surface Characterization of Electro-Assisted Titanium Implants: A Multi-Technique Approach. *Materials* **2020**, *13*, 705. [[CrossRef](#)] [[PubMed](#)]
70. Li, S.; Yu, W.; Zhang, W.; Zhang, G.; Yu, L.; Lu, E. Evaluation of highly carbonated hydroxyapatite bioceramic implant coatings with hierarchical micro-/nanorod topography optimized for osseointegration. *Int. J. Nanomed.* **2018**, *13*, 3643–3659. [[CrossRef](#)]
71. Lotz, E.M.; Olivares-Navarrete, R.; Berner, S.; Boyan, B.D.; Schwartz, Z. Osteogenic response of human MSCs and osteoblasts to hydrophilic and hydrophobic nanostructured titanium implant surfaces. *J. Biomed. Mater. Res. A* **2016**, *104*, 3137–3148. [[CrossRef](#)]
72. Ma, R.; Tang, S.; Tan, H.; Qian, J.; Lin, W.; Wang, Y.; Liu, C.; Wei, J.; Tang, T. Preparation, Characterization, In Vitro Bioactivity, and Cellular Responses to a Polyetheretherketone Bioactive Composite Containing Nanocalcium Silicate for Bone Repair. *ACS Appl. Mater. Interfaces* **2014**, *6*, 12214–12225. [[CrossRef](#)]
73. AbouAitah, K.; Stefanek, A.; Higazy, I.M.; Janczewska, M.; Swiderska-Sroda, A.; Chodara, A.; Wojnarowicz, J.; Szałaj, U.; Shahein, S.A.; Aboul-Enein, A.M.; et al. Effective Targeting of Colon Cancer Cells with Piperine Natural Anticancer Prodrug Using Functionalized Clusters of Hydroxyapatite Nanoparticles. *Pharmaceutics* **2020**, *12*, 70. [[CrossRef](#)] [[PubMed](#)]
74. Padmanabhan, V.P.; Kulandaivelu, R.; Santhana Panneer, D.; Vivekananthan, S.; Sagadevan, S.; Anita Lett, J. Microwave synthesis of hydroxyapatite encumbered with ascorbic acid intended for drug leaching studies. *Mater. Res. Innov.* **2019**, 1–8. [[CrossRef](#)]

75. Guillot, R.; Pignot-Paintrand, I.; Lavaud, J.; Decambren, A.; Bourgeois, E.; Josserand, V.; Logeart-Avramoglou, D.; Viguier, E.; Picart, C. Assessment of a polyelectrolyte multilayer film coating loaded with BMP-2 on titanium and PEEK implants in the rabbit femoral condyle. *Acta Biomater.* **2016**, *36*, 310–322. [[CrossRef](#)]
76. Min, J.; Choi, K.Y.; Dreaden, E.C.; Padera, R.F.; Braatz, R.D.; Spector, M.; Hammond, P.T. Designer Dual Therapy Nanolayered Implant Coatings Eradicate Biofilms and Accelerate Bone Tissue Repair. *ACS Nano* **2016**, *10*, 4441–4450. [[CrossRef](#)]
77. Yaprakci, V.; Erdemli, O.; Kayabolen, A.; Tezcaner, A.; Bozkurt, F.; Keskin, D. In vitro/in vivo comparison of cefuroxime release from poly(ϵ -caprolactone)-calcium sulfate implants for osteomyelitis treatment. *Biotechnol. Appl. Biochem.* **2013**, *60*, 603–616. [[CrossRef](#)] [[PubMed](#)]
78. Nandi, S.K.; Kundu, B.; Mukherjee, P.; Mandal, T.K.; Datta, S.; De, D.K.; Basu, D. In vitro and in vivo release of cefuroxime axetil from bioactive glass as an implantable delivery system in experimental osteomyelitis. *Ceram. Int.* **2009**, *35*, 3207–3216. [[CrossRef](#)]
79. Niu, X.; Sun, L.; Zhang, X.; Sun, Y.; Wang, J. Fabrication and antibacterial properties of cefuroxime-loaded TiO₂ nanotubes. *Appl. Microbiol. Biotechnol.* **2020**, *104*, 2947–2955. [[CrossRef](#)]
80. Mäkinen, T.J.; Veiranto, M.; Lankinen, P.; Moritz, N.; Jalava, J.; Törmälä, P.; Aro, H.T. In vitro and in vivo release of ciprofloxacin from osteoconductive bone defect filler. *J. Antimicrob. Chemother.* **2005**, *56*, 1063–1068. [[CrossRef](#)]
81. Stevanović, M.; Djošić, M.; Janković, A.; Kojić, V.; Vukašinović-Sekulić, M.; Stojanović, J.; Odović, J.; Crevar Sakač, M.; Kyong Yop, R.; Mišković-Stanković, V. Antibacterial graphene-based hydroxyapatite/chitosan coating with gentamicin for potential applications in bone tissue engineering. *J. Biomed. Mater. Res. Part A* **2020**, *108*, 2175–2189. [[CrossRef](#)]
82. Giacomini, D.; Torricelli, P.; Gentilomi, G.A.; Boanini, E.; Gazzano, M.; Bonvicini, F.; Benetti, E.; Soldati, R.; Martelli, G.; Rubini, K.; et al. Monocyclic β -lactams loaded on hydroxyapatite: New biomaterials with enhanced antibacterial activity against resistant strains. *Sci. Rep.* **2017**, *7*, 2712. [[CrossRef](#)]
83. Geng, Z.; Cui, Z.; Li, Z.; Zhu, S.; Liang, Y.; Liu, Y.; Li, X.; He, X.; Yu, X.; Wang, R.; et al. Strontium incorporation to optimize the antibacterial and biological characteristics of silver-substituted hydroxyapatite coating. *Mater. Sci. Eng. C* **2016**, *58*, 467–477. [[CrossRef](#)] [[PubMed](#)]
84. Brohede, U.; Forsgren, J.; Roos, S.; Mihranyan, A.; Engqvist, H.; Strømme, M. Multifunctional implant coatings providing possibilities for fast antibiotics loading with subsequent slow release. *J. Mater. Sci. Mater. Med.* **2009**, *20*, 1859–1867. [[CrossRef](#)] [[PubMed](#)]